J Mater Sci (2014) 49:5856–5865
DOI 10.1007/s10853-014-8296-y

Interface modification of clay and graphene platelets reinforced epoxy nanocomposites: a comparative study

Izzuddin Zaman · Bukhari Manshoor · Amir Khalid · Qingshi Meng · Sherif Araby

Received: 3 February 2014 / Accepted: 2 May 2014 / Published online: 21 May 2014

Abstract The interface between the matrix phase and dispersed phase of a composite plays a critical role in influencing its properties. However, the intricate mechanisms of interface are not fully understood, and polymer nanocomposites are no exception. This study compares the fabrication, morphology, and mechanical and thermal properties of epoxy nanocomposites tuned by clay layers (denoted as *m*-clay) and graphene platelets (denoted as *m*-GP). It was found that a chemical modification, layer expansion and dispersion of filler within the epoxy matrix resulted in an improved interface between the filler material and epoxy matrix. This was confirmed by Fourier transform infrared spectroscopy and transmission electron microscope. The enhanced interface led to improved mechanical properties (i.e. stiffness modulus, fracture toughness) and higher glass transition temperatures (T_g) compared with neat epoxy. At 4 wt% *m*-GP, the critical strain energy release rate G_{1c} of neat epoxy improved by 240 % from 179.1 to 608.6 J/m^2 and T_g increased from 93.7 to 106.4 °C. In contrast to *m*-clay, which at 4 wt%, only improved the G_{1c} by 45 % and T_g by 7.1 %. The higher level of improvement offered by *m*-GP is attributed to the strong interaction of graphene sheets with epoxy because the covalent bonds between the carbon atoms of graphene sheets are much stronger than silicon-based clay.

I. Zaman (✉) · B. Manshoor · A. Khalid
Faculty of Mechanical and Manufacturing Engineering, Universiti Tun Hussein Onn Malaysia, Parit Raja, 86400 Batu Pahat, Johor, Malaysia
e-mail: izzuddin@uthm.edu.my
URL: http://community.uthm.edu.my/izzuddin

Q. Meng · S. Araby
School of Engineering, University of South Australia, Mawson Lakes, SA 5095, Australia

Introduction

Epoxy resins are widely used, with applications in adhesion, biotechnology and electronics and in the automotive and aerospace industries. They possess excellent adhesive and thermal properties and high strength. However, epoxy resins have a low fracture toughness leading to poor crack resistance, and this is attributed to their highly cross-linked molecular structure.

A myriad of attempts has been made at improving the fracture toughness of epoxy resins using inorganic particles [1–4]. In some cases, epoxy composites contained between 10 and 30 wt% of filler material. This high weight ratio increased the weight of the composite considerably and was a detriment to other advantageous properties of the polymer matrix [5–9]. In recent developments, polymer nanocomposites containing layer-structured particles such as clay montmorillonite (MMT) and graphene showed improvements in fracture toughness. This is because of the large surface area of clay and graphene and their inexpensive fabrication [10–13]. However, research on improving the interface between epoxy resins and layer-structured fillers is still in its stages of infancy. The hypothesis is that a strong interface between matrix and filler will result in improved mechanical and thermal properties of composites.

Montmorillonite is a 2:1 clay having two silica tetrahedral sheets sandwiching an octahedral sheet, with thickness usually around 0.96 nm (see Fig. 1a). Depending on the degree of hydration, the layer spacing between platelets ranges from 1.1 to 1.33 nm. Being hydrophilic and having the ability to swell, MMT allows H_2O molecules to intercalate between its layers and this forms a stable suspension in water [14]. These properties, however, make them extremely difficult to exfoliate in organic systems. Therefore, MMT is usually modified by surfactants to improve its compatibility

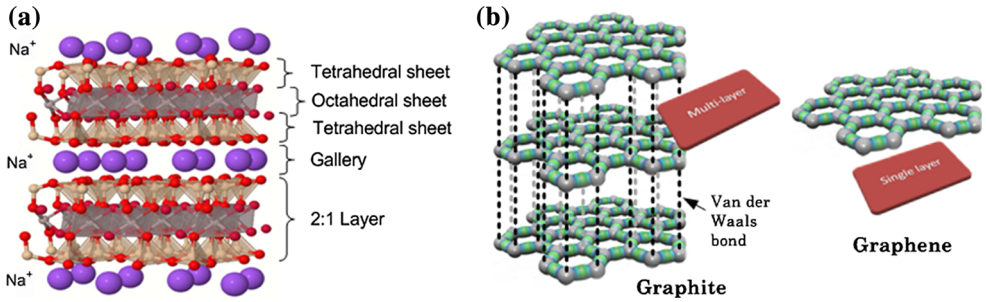

Fig. 1 Atomic structure of **a** MMT clay and **b** graphite

with hydrophobic organic polymers and used in nanocomposites. On the other hand, graphene is a one-atom-thick sheet of carbon atoms that are arranged in a hexagonal pattern (see Fig. 1b). By the weak bonding of Van der Waals forces, sheets of graphene stack together in nature forming graphite in which the inter-planar spacing is 0.335 nm. A single-layer graphene has exceptional mechanical properties with a Young's modulus of 1 TPa and an intrinsic tensile strength of 130 GPa [15]. They exhibit immense potential as nanofillers since they are chemically stable, abundant in nature (as graphite) and hence cheap.

Based on the arrangement of the layer-structured filler in the polymer matrix, two kinds of phase structures exist, i.e. exfoliated and intercalated. Research has revealed that exfoliated structures result in a higher degree of improvement in mechanical properties. Three steps to improve the exfoliation of a filler and its dispersion in a polymer matrix involve (1) increasing the layer spacing of a filler through suspension in a solvent or sonication or by thermal shock in the case of graphene [16, 17]; (2) using surfactants to chemically modify the surface of the filler to ensure its bridging with the polymer matrix [18, 19]; and (3) the creation of physical entanglement between the layered filler and polymer matrix [20]. In the case of clay nanocomposites, small weight ratios of filler in the order of a few per cent have been found to improve mechanical properties and heat and fire resistance, and liquid and gas barrier properties. Messersmith and Giannelis [21] who pioneered research in epoxy/clay nanocomposites relied heavily on intercalation while exfoliation of clay was brought about by the curing of the polymer. Recent approaches in epoxy/graphene nanocomposites such as one pursued by Miller have incorporated a coupling agent which built covalent bonds between the filler and matrix. This led to the Young's modulus being improved by 50 % with a filler content of just 1 % [22].

Despite the significant number of research papers published over the past 15 years describing epoxy/clay and epoxy/graphite, the understanding of the role of interface of these layer-structured fillers still remains unclear. Although research is still in its infancy, initial findings have shown that interface-tuned nanocomposites are a promising method for enhancing other nanocomposites properties [23–26]. In this study, we compared the properties of epoxy nanocomposites by interface-tuning with clay layers and graphene platelets (GP). This includes investigating the essence of modification of both types of filler surface on the filler–polymer interface through observing the property improvements. It concludes how the interface controls the property improvement by selecting the right filler with the suitable modification to get the demanded property. In this case, the interface of the systems was analysed through Fourier transform infrared spectroscopy (FTIR), X-ray diffraction (XRD), transmission electron microscope (TEM) and scanning electron microscope (SEM). The effects on mechanical properties, fracture toughness and thermal dynamic properties were also explained.

Experimental

Materials

The matrix used was an epoxy resin, diglycidyl ether of bisphenol A (DGEBA, Araldite-F) with an epoxide equivalent weight of 182–196 g/equiv. It was supplied by Ciba-Geigy, Australia. The hardener used was polyoxypropylene (Jeffamine® J230), and it was supplied by Huntsman. Sodium montmorillonite was purchased by Southern Clay Products along with a cation exchange capacity (CEC) of 85 mequiv/100 g. The acid-treated graphite oxide (Ashbury 3494) was supplied by Ashbury Carbons, Ashbury, NJ. The solvents 4,4′-methylene diphenyl diisocyanate (MDI) and tetrahydrofuran (THF) were purchased from Sigma-Aldrich. The surfactant Jeffamine® XTJ502 (XTJ) was provided by Huntsman.

Modification of clay surface

Ten gram of clay was dispersed in 2 kg of boiling deionized water using a uniform stirring method for 10 min on the mechanical stirrer. Separately, a mixture was created by dissolving a stoichiometric amount of XTJ in 200 g of water and then adding 10 g of hydrochloric acid (37 wt%, 0.086 mol/ml) to the mixture. The mixture was then stirred

using a glass rod and was slowly added to the clay suspension on the mechanical stirrer at 90 °C for 10 min of uniform stirring. The resulting mixture was organoclay which was then condensed using a rotary vacuum evaporator starting at 80 °C and then increasing to 90 °C for 30 min. The condensed organoclay was separated using a centrifuge. The precipitate of the separated organoclay was repeatedly washed at least three times using acetone, then stirred with a magnetic stirrer, subject to sonication and put through centrifuge again. The washed organoclay was then suspended in 500 ml of acetone to produce a slurry organoclay/acetone suspension which is called *m*-clay.

Modification of graphene surface

Four gram of graphite is pestled in a mortar and then mixed with acetone in a 400 ml metal container. The container was then covered and sonicated for 30 min using an ultrasonic bath with specifications of 200 W and 42 kHz. During sonication, the graphite was split into GP which became suspended in the acetone solvent as reported by Cravatto [27]. A great amount of care was taken to ensure the precipitate remained in the container while the suspension was transferred to a glass beaker. The glass beaker was then covered and stored at room temperature for 2 h to allow the suspended GP to precipitate. The precipitate was then collected and dried. These steps were repeated until the required amount of GP was obtained. Once the required amount of GP was obtained, it was suspended in the solvent THF by sonication. The suspended GP were transferred to a round-bottom flask that attached to a condenser. Using a weight ratio of 0.5 MDI to graphite, small amounts of MDI were dropped into the suspended GP within a span of 3 min while being mixed using a magnetic stirrer. The stirring then continued for 6 h at 80 °C. The modified GP obtained are called *m*-GP.

Synthesis of epoxy/clay nanocomposite

A desired amount of *m*-clay was mixed with DGEBA for 1 h at 55 °C setting the mechanical stirrer at 400 rpm in a round-bottom flask with condenser attached. After mixing, the mixture was transferred to a beaker after which it was mixed again at 300 rpm at 120 °C for 1 h to evaporate the acetone. It was then degassed in a vacuum oven set at 120 °C. After degassing, a stoichiometric amount of curing agent J230 (1:3.3 weight ratio of DGEBA to J230) was added to the mixture and mixed for only 2 min at 50 °C. After mixing, the mixture was degassed again in the vacuum oven for 5 min to remove any trapped bubbles in the mixture. Finally, the degassed mixture was poured into rubber moulds to be cured at 80 °C for 3 h and at 120 °C for another 12 h.

Synthesis of epoxy/m-GP composites

DGEBA was added to the *m*-GP followed by mixing at 600 rpm at 110 °C for around 12–15 h in the round-bottom flask with a condenser. After this, acetone was added after to reduce the viscosity of the mixture to ensure the uniform dispersion of *m*-GP. The acetone was then evaporated by mixing at 100 °C for 1 h, followed by degassing at 120 °C. The mixture was then cooled down to 50 °C before hardener J230 was added. The mixture was mixed for 2 min followed by degassing and then poured into rubber moulds for curing at 80 °C for 3 h and at 120 °C for another 12 h (same as clay).

Characterization

A recording of spectra of neat epoxy with the nanocomposites from 4000 cm^{-1} to 700 cm^{-1} using a minimum of 32 scans was recorded using a Nicolet Avatar 320 FTIR. Also, the FTIR samples were prepared by solution-casting method on the KBr plate.

X-ray diffraction (XRD) was performed using Mini-Materials Analyser (MMA) at room temperature on the sample. The diffractometer was equipped with curved graphite monochromators, tuned to Cu K radiation. The tube voltage applied was at 35 kV with an X-ray power of 1 kW. The diffraction patterns were collected in a reflection mode geometry of between $2\theta = 1.5°–12°$ at a scanning rate of 1°/min.

Two-dimensional images of the internal structure of the nanocomposites were obtained using transmission electron microscopy (TEM). Ultrathin sections of 50 nm are microtomed from bulk samples using the Leica Ultracut S microtome which was equipped with a diamond knife. The microtomes were collected on 200-mesh copper grids. The ultrathin sections were examined using Phillips CM200 TEM at 200 kV accelerating voltage.

The fracture surfaces of compact tension (CT) samples were analysed using scanning electron microscopy (SEM). The fracture surface was coated with a thin layer of platinum and observed using Phillips XL30 FegSEM at an acceleration voltage of 10 kV.

Tensile testing was performed on dumb-bell samples at a strain rate of 0.5 mm/min according to ASTM D-638 to obtain the elastic modulus, ultimate stress and ultimate strain of neat epoxy and its nanocomposites. The tensile tests were performed using the Instron 5567 testing system with a 10 kN load cell and an extensometer. The average interested values of all properties mentioned are recorded from five repetitions of each test. Young's moduli were calculated at a strain range of 0.05–0.15 %.

Compact tension (CT) fracture toughness requires great care to produce an instantly propagated crack [28]. The

main difficulty was in producing the instantly propagated crack due to restrictions on cross-sectional area. The CT samples were approximately 30 mm wide and 5 mm thick in accordance with ASTM D-5045. Using a sharp razor blade, an instantly propagated crack was produced on each CT sample. The cracked CT samples were tested using the Instron 5567 system with a 2 kN load cell at a strain rate of 0.5 mm/min. The fracture toughness properties are expressed by a stress intensity factor, K_{1C}, and critical strain energy release rate, G_{1C}. The G_{1C} is calculated by using the following equation:

$$G_{1C} = \frac{K_{1C}(1 - v^2)}{E} \quad (1)$$

where E is Young's modulus and v is Poisson ratio.

In each of the aforementioned mechanical properties, at least three samples for each fraction were tested and the average value was used in the graphs. The standard deviation is calculated and indicated by the range bars over the graphs.

The glass transition temperature of the nanocomposites and neat epoxy were obtained using Dynamic Mechanical Analyser 2980 (TA Instrument, Inc., USA) tested at 1 Hz. The rectangular sample that was tested had dimensions of 3.0 × 6.0 × 40.0 mm. The sample was clamped using a single cantilever clamp with supporting span of 20 mm and torque of 1 Nm. The scanning was done from 50 to 120 °C and recorded at 2 s/point.

Results and discussion

Chemical structure characterization

Figure 2 shows the FTIR spectra of sodium clay, clay modified by XTJ502 (*m*-clay), raw graphite and grapheme platelet modified by MDI (*m*-GP). The FTIR analysis was performed to confirm the grafting of surfactant onto the layer-structured fillers after modification. The characteristic bands of sodium clay showed dominant absorption from 991 to 1045 cm^{-1} which was attributed to the Si–O band in-plane stretching of clay; the absorption at 1636 cm^{-1} due to the O–H deformation of entrapped water; and the absorption at 3620 cm^{-1} assigned to O–H stretching of structure hydroxyl group of the clay [29, 30]. After clay was modified by surfactant XTJ502, new characteristic absorption bands are observed at 1246, 1456 and 2900 cm^{-1} contributed by C–O band stretching, $–CH_2–$ groups and –CH– groups [31], respectively. This spectrum confirmed the grafting of XTJ502 molecules onto the clay surface through cationic exchange as was described in "Modification of clay surface" section.

On the contrary, graphite consists of carbon atoms and displays a different spectrum to clay where it reduces

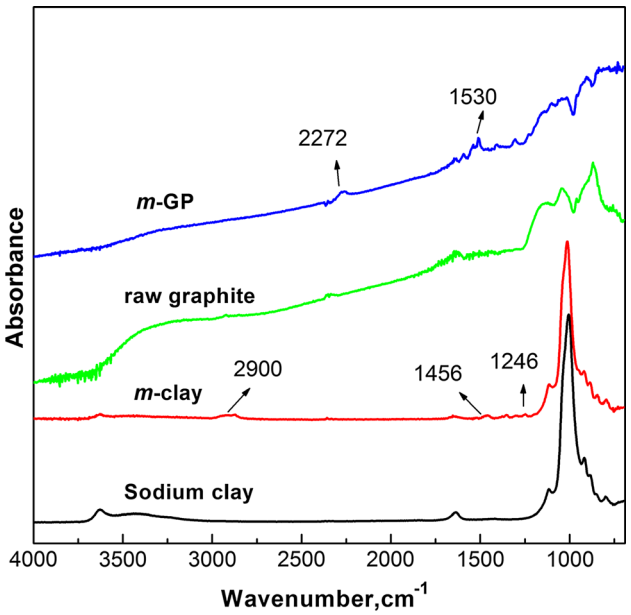

Fig. 2 FTIR spectra of sodium clay, *m*-clay, raw graphite and *m*-GP (graphs are *vertically* shifted for clarity)

against wave number. Since the raw graphite used in the study was treated with acid, strong absorptions of acid were expected. The characteristic bands of raw graphite show absorption at 2327 cm^{-1} and a band between 3304 and 3500 cm^{-1} attributed to the presence of –OH group; absorptions at 1650 and 873 cm^{-1} correspond to the stretching vibration of –C=O and –C–O–, respectively, which imply the existence of carboxyl group; and the absorption at 1043 and 1144 cm^{-1} indicates the presence of the –S=O group. Upon modification by 4,4′-methylene diphenyl diisocyanate (MDI), the absorption intensity of –OH group decreases, which implies that a reaction involving the –OH groups has occurred. As mentioned in "Modification of graphene surface" section, during modification, the –OH– groups of GP reacted with MDI. Two new absorption peaks appear in the *m*-GP spectrum: (1) absorption at 2272 cm^{-1} due to the isocyanate –N=C=O stretching and (2) absorption at 1530 cm^{-1} corresponding to the vibration of CNH groups [32]. Bearing similarity to clay, this result indicates that the MDI was grafted to GP through. This implies that the grafting of surfactant molecules onto layer-structured fillers was successful.

Structural characterization

The XRD diffractions spectra of sodium clay, *m*-clay and epoxy/*m*-clay nanocomposite are shown in Fig. 3. A diffraction peak at $2\theta = 7.36°$ is assigned to the [001] lattice spacing of sodium clay [33], which corresponds to a d-spacing of 12 Å. Upon modification, the *m*-clay showed

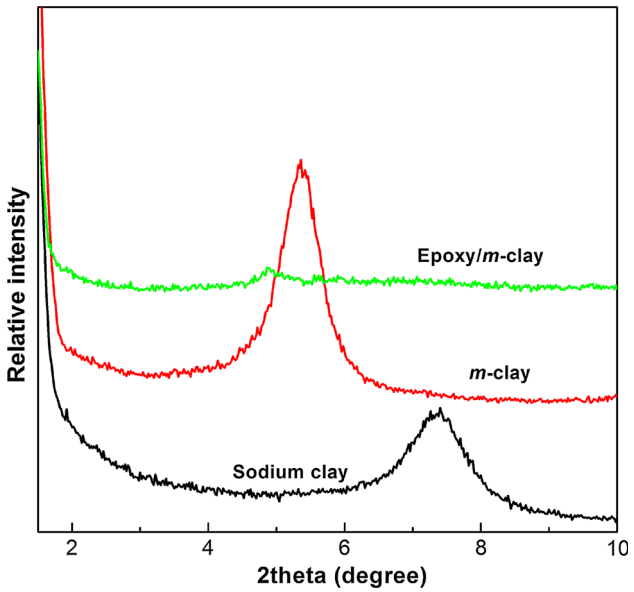

Fig. 3 XRD patterns of sodium clay, *m*-clay and 2.5 wt% epoxy/*m*-clay nanocomposite

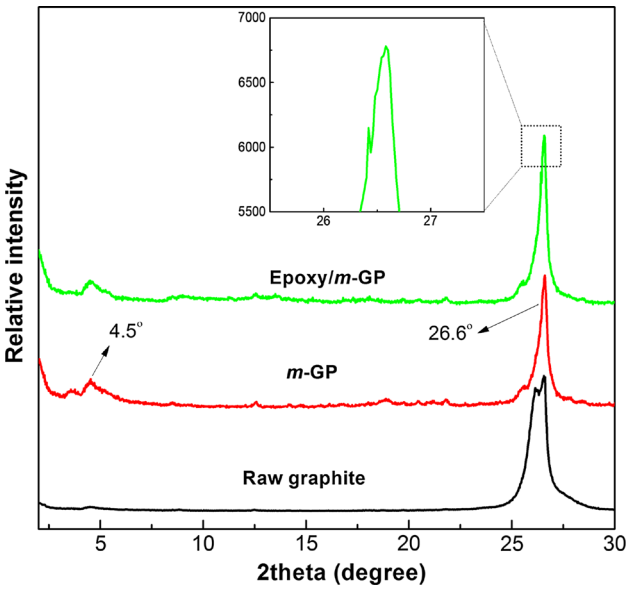

Fig. 4 XRD patterns of raw graphite, *m*-GP and 2.5 wt% epoxy/*m*-GP nanocomposite

a strong diffraction peak and shifting to lower angles. This result shows that there is an increase in layer spacing to 16.5 Å. It confirms the grafting of XTJ502 molecules onto the clay surface as was also indicated by FTIR analysis. However, the diffraction peak at $2\theta = 4.98°$ of *m*-clay almost disappeared when 2.5 wt% epoxy/*m*-clay nanocomposite was fabricated, suggesting a further expansion of the clay galleries. This is because one end of the *m*-clay amine group reacts with the epoxide group, bringing a large number of epoxy molecules into the clay galleries resulting in exfoliation.

Figure 4 shows the XRD patterns of raw graphite, *m*-GP and epoxy/*m*-GP nanocomposites. For raw graphite, a double peak was observed at $2\theta = 26.2°$ and 26.6°, which indicates the layer spacing of graphite was increased by intercalates during manufacturing. After modification by MDI, the diffraction pattern broadens and shows two distinct peaks at $2\theta = 26.6°$ and 4.5° corresponding to layer spaces of 3.4 Å and 19.6 Å, respectively. This implies that some sheets of GP have expanded during its modification with MDI. Although the difference between the diffraction peaks of GP and clay is insignificant, the modification of GP has reduced the regularity of its layer stacking and this is inferred from the broader diffraction pattern of GP. When *m*-GP are compounded with epoxy, the diffraction of the nanocomposite shows a broader peak with a small shoulder as shown in the enlargement in Fig. 4. This is attributed to the modification facilitates the interaction of epoxy molecules into the layer spacing of *m*-GP, so that epoxy resin and hardener J230 could reacts with grafted MDI molecules. The chemical modification of clay and graphene forms *m*-clay and *m*-GP, respectively, in which both possess better interfaces with epoxy as compared to their unmodified forms. This enhanced interface could lead to improvements in morphology, mechanical properties and thermal dynamic properties of epoxy nanocomposites.

Morphology characterization

In this study, TEM and SEM were employed to characterize the morphology of the fabricated nanocomposites. Although some preliminary results of XRD proved the exfoliation and intercalation of clay layers and graphene nanosheets within the polymer matrix, TEM and SEM would provide valuable information with regard to the dispersion of the individual layers of filler material, interfacial interaction and an understanding of the structure–property link at the atomistic level.

TEM micrographs

TEM micrographs of epoxy/*m*-clay and epoxy/*m*-GP nanocomposites are shown in Fig. 5. It is clear from Fig. 5a, at 100-nm scale, that the clay platelets are arranged in a random and disorderly fashion with the formation of a few clusters in the epoxy matrix. The dark lines correspond to clay layers, some of which are folded and curled up, while the light area corresponds to the epoxy matrix. Some regions of epoxy are visible due to the inhomogeneous dispersion of clay layers at the molecular level. In contrast to epoxy/*m*-clay nanocomposites, the cluster size of GP in epoxy/*m*-GP nanocomposites is larger and this is shown in Fig. 5b. It appears that single and stacked GP were found

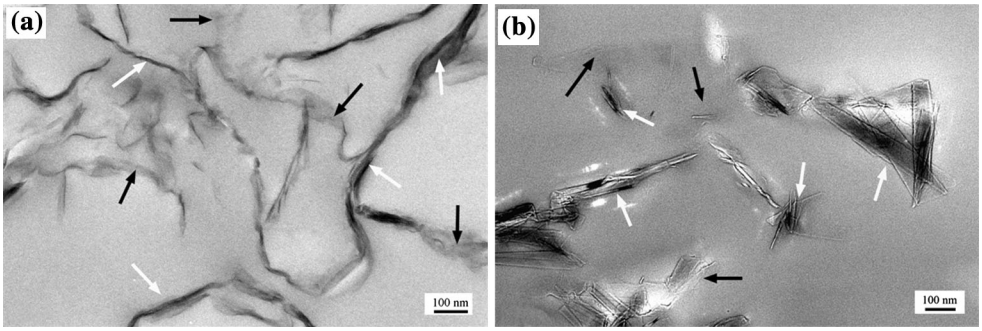

Fig. 5 Comparison of TEM micrographs of **a** 2.5 wt% epoxy/*m*-clay nanocomposite, **b** 2.5 wt% epoxy/*m*-GP nanocomposite. The *white arrows* indicate intercalated layers, while *black arrows* refer to exfoliated arrows

folded due to a reduction of thickness of platelets. During curing, the MDI that was grafted to the GP reacted with the hardener J230, which separated the platelets into thinner layers. This lead to more folds in the GP in order to reduce configurational entropy [34]. From TEM analysis, it can be concluded that both nanocomposites show improvements in the interface which have been brought about by modification. It is also observed that *m*-clay shows better dispersion and layer exfoliation than *m*-GP in the epoxy matrix. This is because the long-chain molecules of XTJ502 penetrate the clay layers, pushing them further apart during curing process of epoxy and hardener [35].

SEM micrographs

The fracture surface of tensile samples as shown in Figs. 6, 7 and 8 provides critical information on the fracture mechanisms of neat epoxy, and epoxy/*m*-clay and epoxy/*m*-GP nanocomposites. From Fig. 6a, it is seen that the fracture surface of neat epoxy shows a smooth surface with hackles (river-marking) at regions of deformation. The magnified micrograph in Fig. 6b shows the hackles more clearly, and this is a characteristic of the brittle failure of neat epoxy [36].

The fracture surface behaviour of epoxy/*m*-clay nanocomposites is rougher compared to that of neat epoxy as shown in Fig. 7a. This is indicative of the ductile nature of epoxy/*m*-clay nanocomposites which is attributed to a stronger interface. From the magnified micrograph of Fig. 7b, it is noted that clusters with diameters in range of 4–5 μm are visible and dispersed almost uniformly throughout the epoxy matrix in accordance with the information yielded by the TEM micrographs. Some clay layers are found broken and cracked in between the epoxy/clay interface (as shown by the arrows), indicating that crack path deflection and microcracking are the toughening mechanisms of epoxy/*m*-clay nanocomposite.

Figure 8a shows the tensile fracture surface of an epoxy/*m*-GP nanocomposite. The blended epoxy/*m*-GP appear to be dense, indicating a strong interaction between the epoxy and graphene sheets. Clusters of stacked GP as indicated by the arrows are observed in the micrograph. The magnified micrograph in Fig. 8b shows features such as voids, trenches, layer breakage and microcracks. The appearance of trenches indicates a high degree of surface deformation, which is responsible for the absorption of a large amount of fracture energy.

Mechanical properties characterization

Tensile properties

Figure 9 shows the Young's modulus and tensile strength of neat epoxy, *m*-clay nanocomposites and *m*-GP nanocomposites at 1–4 wt%. The Young's modulus of neat epoxy significantly increases with the increase in filler concentration, while the tensile strength was found to drop. The significant improvement in stiffness is explained by restriction of polymer chain mobility through sharing the stress between filler and matrix, and thus creates shear deformation. Clay and graphene have much higher stiffness values than the epoxy. The drop in tensile strength is attributed to the debonding of particles, voids and failure in some clusters, and this is verified by SEM and TEM results.

Epoxy/*m*-clay nanocomposites show a greater improvement in Young's modulus and lower reduction of tensile strength than epoxy/*m*-GP nanocomposites. A total of 4 wt% of *m*-clay increased the modulus of neat epoxy by 31 % from 2.69 to 3.54 GPa, while at the same weight concentration, the modulus of epoxy/*m*-GP only increased by 22 % to 3.27 GPa. This was in spite of the fact that graphene possesses a higher specific area of 2600 $m^2\ g^{-1}$ and is stiffer than clay (up to 1000 $m^2\ g^{-1}$). This is because the clay layers are exfoliated to a much higher degree than graphene while graphene nanosheets remained stacked and formed large clusters in the matrix (as seen in Fig. 5). Another reason is that the long-chain molecules of XTJ502

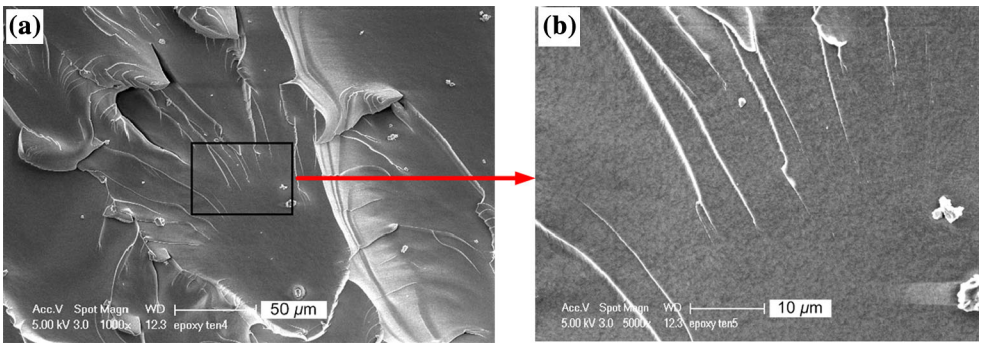

Fig. 6 SEM micrographs of tensile fracture surface of neat epoxy

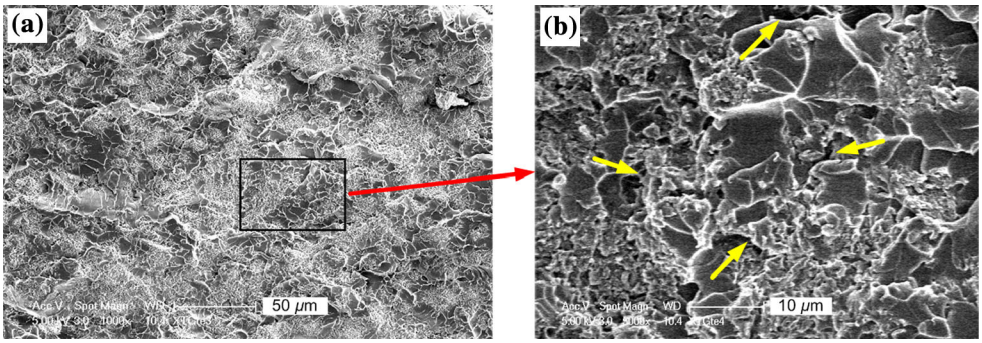

Fig. 7 SEM micrographs of tensile fracture surface of 2.5 wt% epoxy/*m*-clay nanocomposite

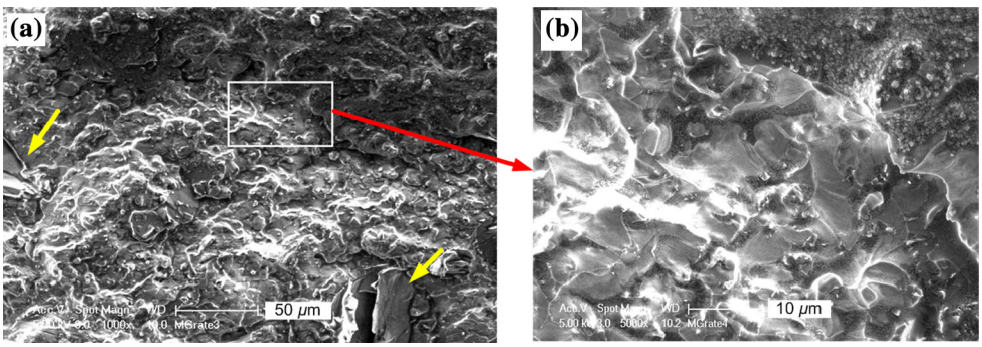

Fig. 8 SEM micrographs of tensile fracture surface of 2.5 wt% epoxy/*m*-GP nanocomposite

(M_w of 2000 g/mol) enable physical entanglement between the clay layers and epoxy, leading to an improvement in stiffness. In contrast, *m*-GP nanocomposites are modified by the short-chained molecules MDI which has a molecular weight of just 250 g/mol.

Fracture properties

Figure 10 shows the fracture toughness, K_{1c}, and critical energy release rate, G_{1c}, of neat epoxy, epoxy/*m*-clay and epoxy/*m*-GP nanocomposites. As was the case with tensile properties, the fracture toughness of epoxy improved significantly with the addition of the nanolayered fillers. At low content of 1 wt%, epoxy/*m*-clay shows higher fracture toughness, and a steady increase in toughness with weight concentration is observed in epoxy/*m*-GP. At 4 wt%, epoxy/*m*-GP nanocomposites display higher toughness than epoxy/*m*-clay, where the K_{1c} of neat epoxy increases by 103 % from 0.653 MPa $m^{0.5}$ to 1.326 MPa $m^{0.5}$. At the same fraction, *m*-clay improves the K_{1c} by only 38 % to 0.90 MPa $m^{0.5}$. The fracture toughness of epoxy/*m*-clay reached a peak at a weight concentration of 2.5 wt%. A similar pattern was observed for G_{1c}. The main toughening mechanism for epoxy/clay nanocomposites is interface debonding. When loaded, the *m*-clay layers carry and transfer most of the stress to relieve stress concentration on

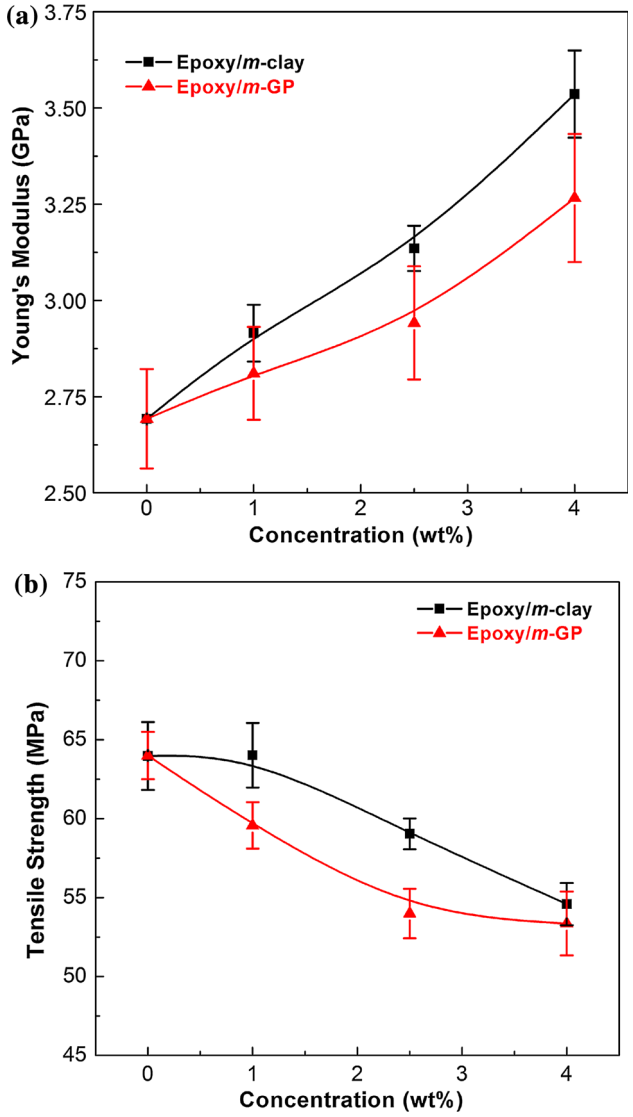

Fig. 9 Young's modulus and tensile strength of epoxy/*m*-clay and epoxy/*m*-GP nanocomposites

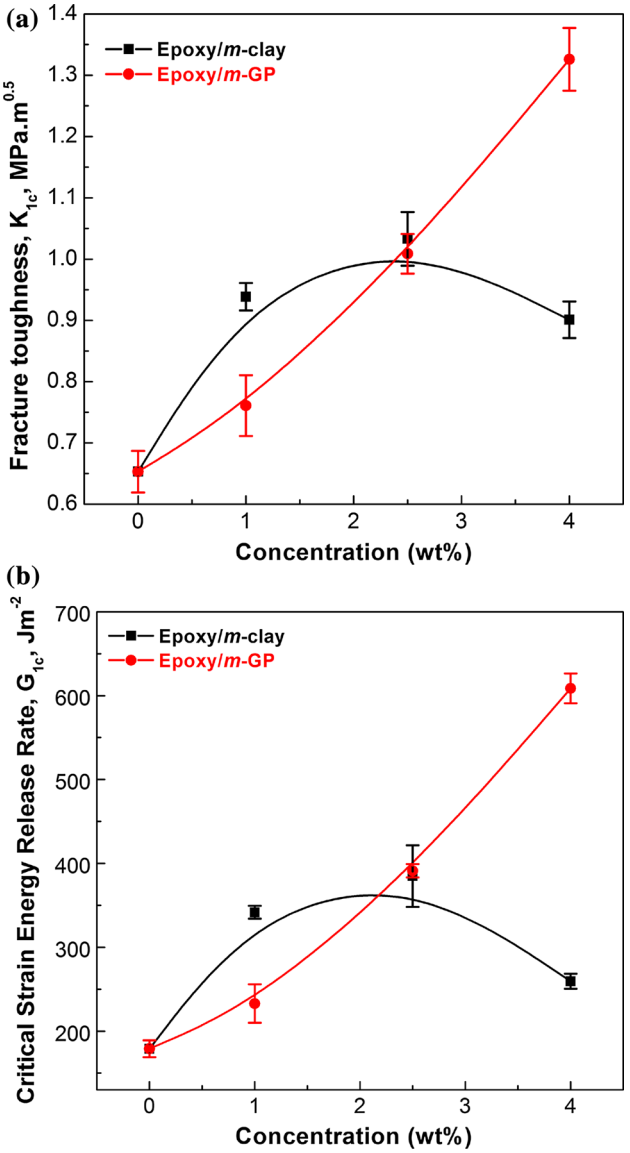

Fig. 10 Fracture toughness and energy release rate of epoxy/*m*-clay and epoxy/*m*-GP nanocomposites

the crack and absorb fraction energy. GP provide greater toughening because the covalent bonds between the carbon atoms of graphene sheets are much stronger. It is also more compatible with hydrophobic polymer matrices than clay layers due to its carbon-based composition. Clay has a silicon-based composition.

Thermal dynamic characterization

Figure 11 presents the damping behaviour of neat epoxy, epoxy/*m*-clay and epoxy/*m*-GP nanocomposites at 1–4 wt%. The glass transition temperature, T_g, is determined from the midpoints of the corresponding glass transition regions and is the parameter that will be analysed in the study. The glass transition of the resin increased when the reinforced layer-structured fillers were combined with the epoxy matrix. This is because (1) high specific area of the layered nanostructure poses barriers to the vibration of matrix molecules through the T_g region—causing longer relaxation time for cross-linked chains to rearrange themselves and subsequently resulting in higher T_g—and (2) the strong coupling in vibration modes at the filler–polymer interface provides resistance to the vibration of matrix chains at T_g due to the bridging of layer-structured filler and epoxy matrix.

From the graph, it can be seen that *m*-GP nanocomposites show a higher T_g compared to *m*-clay nanocomposites. In fact, at 2.5 wt% *m*-GP, T_g of epoxy reaches up maximum to 108.6 °C, giving an increment of 11.7 °C higher than that of neat epoxy. This result confirms the strong interface of

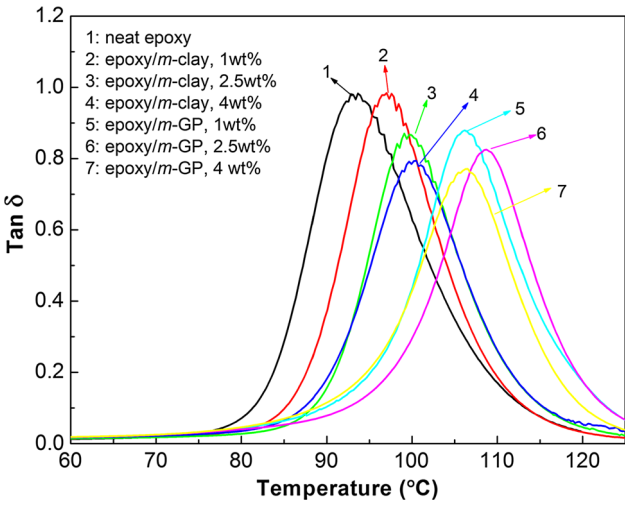

Fig. 11 Thermal dynamic properties of epoxy/*m*-clay and epoxy/*m*-GP nanocomposites

epoxy/*m*-GP nanocomposites, which seems to correlate with the fracture toughness results. As proved from FTIR results, for *m*-GP, the strong interaction of surface-grafted MDI by reaction of –O– groups with epoxy and hardener J230 enables a strong interface to confine the polymer chain vibration at T_g. In spite of the fact that the *m*-GP are not completely exfoliated, its dispersion as small clusters was found uniformly throughout the matrix as demonstrated in the TEM. This structure traps epoxy chains between cluster–cluster distances leading to a decrease in the chain mobility which in turn increases T_g. This result is in accordance with findings in our previous papers [17–19], which dictate that a higher interface strength results in higher T_g for epoxy nanocomposites. At 4 wt%, a decrease was observed in the T_g of epoxy/*m*-GP. This could be attributed to larger particle sizes and the lower surface area of GP with the increase in filler content. These factors would reduce the reinforcing efficiency of the filler and associated interface that lead to the decreased T_g.

Conclusions

The epoxy/layered structure nanocomposites were successfully prepared using clay and GP as reinforcing fillers. In this paper, the interaction between the epoxy matrix and both layer-structured fillers was compared, and detailed discussions were made relating to the morphology, mechanical properties, fracture toughness and thermal dynamic properties of nanocomposites. The use of the surfactants, XTJ502 and MDI with clay and graphene, respectively, (containing two reactive sites) enabled the integration of the fillers with the epoxy matrix. This concept of interface enhancement will lead to significant improvements in mechanical and thermal dynamic properties of nanocomposites. It was remarkable to see that *m*-GP toughened the epoxy by a fourfold increase of fracture energy release rate at 4 wt% in comparison with the performance of *m*-clay which only enabled a onefold increase at the same fraction. Upon compounding 2.5 wt% *m*-GP, the glass transition temperature of neat epoxy was increased from 94.7 to 108.6 °C. This is attributed to (1) the covalent bonds between the carbon atoms of graphene sheets are much stronger in comparison with the ionic bonds of silicon-based clay and (2) the higher compatibility of graphene with the hydrophobic epoxy matrix. Nevertheless, both nanocomposites have shown significant improvements in mechanical performance, especially the fracture toughness of neat epoxy, which could have wide applications in engineering.

Acknowledgements I.Z. thanks Ministry of Higher Education Malaysia and Universiti Tun Hussein Onn Malaysia for the award of scholarship. Jeffamine was kindly provided courtesy of Huntsman (Singapore). The authors thank B Wade, L Waterhouse and J Terlet for technical support at Adelaide Microscopy.

References

1. Njuguna J, Pielichowski K, Alcock JR (2007) Epoxy-based fibre reinforced nanocomposites. Adv Eng Mater 9:835–847
2. Becker O, Simon GP (2005) Epoxy layered silicate nanocomposites. Adv Polym Sci 179:29–82
3. Kinloch AJ, Taylor AC (2003) Mechanical and fracture properties of epoxy/inorganic micro- and nano-composites. J Mater Sci Lett 22:1439–1441
4. Ma J, La LTB, Zaman I et al (2011) Fabrication, structure and properties of epoxy/metal nanocomposites. Macromol Mater Eng 296:465–474
5. Amdouni N, Sautereau H, Gerard JF (1992) Epoxy composites based on glass-beads. 2. Mechanical properties. J Appl Polym Sci 46:1723–1735
6. Ma J, Mo M-S, Du X-S, Dai S-R, Luck I (2008) Study of epoxy toughened by in situ formed rubber nanoparticles. J Appl Polym Sci 110:304–312
7. Kinloch A, Mohammed RD, Taylor AC, Eager C, Sprenger S, Egan D (2006) The effect of silica nano particles and rubber particles on the toughness of multiphase thermosetting epoxy polymers. J Mater Sci 41:1293
8. Ozturk A, Kaynak C, Tincer T (2001) Effects of liquid rubber modification on the behaviour of epoxy resin. Eur Polym J 37: 2353–2363
9. Choi J, Yee AF, Laine RM (2004) Toughening of cubic silsesquioxane epoxy nanocomposites using core shell rubber particles; a three component hybrid system. Macromolecules 37: 3267–3276
10. Jia XT, Campos-Delgado J, Terrones M, Meunier V, Dresselhaus MS (2011) Graphene edges: a review of their fabrication and characterization. Nanoscale 3:86–95
11. Goettler LA, Lee KY, Thakkar H (2007) Layered silicate reinforced polymer nanocomposites: development and applications. Polym Rev 47:291–317
12. Ratna D, Manoj N, Varley R, Singh Raman R, Simon GP (2003) Clay reinforced epoxy nanocomposites. Polym Int 52:1403–1407

13. Zaman I, Manshoor B, Khalid A, Araby S (2014) From clay to graphene for polymer nanocomposites—a survey. J Polym Res 21:429
14. Morvan M, Espinat D, Lambard J, Zemb T (2002) Ultrasmall-angle and small-angle X-ray scattering of smectite clay suspensions. Colloids Surf A 82:193–203
15. Lee C, Wei XD, Kysar JW, Hone J (2008) Measurement of the elastic properties and intrinsic strength of monolayer graphene. Science 321:385–388
16. Ma J, Xu J, Ren JH, Yu ZZ, Mai YW (2003) A new approach to polymer/montmorillonite nanocomposites. Polymer 44:4619–4624
17. Zaman I, Phan TT, Kuan H-C et al (2011) Epoxy/graphene platelets nanocomposites with two levels of interface strength. Polymer 52:1603–1611
18. Zaman I, Le Q, Kuan HC et al (2011) Interface-tuned epoxy/clay nanocomposites. Polymer 52:497–504
19. Zaman I, Kuan HC, Meng Q et al (2012) A facile approach to chemically modified graphene and its polymer nanocomposites. Adv Funct Mater 22:2735–2743
20. Araby S, Zaman I, Meng Q et al (2013) Melt compounding with graphene to develop functional, high-performance elastomers. Nanotechnology 24:165601–165614
21. Messersmith PB, Giannelis EP (1994) Synthesis and characterisation of layered silicate–epoxy nanocomposites. Chem Mater 6:1719–1725
22. Miller SG, Bauer JL, Maryanski MJ et al (2010) Characterization of epoxy functionalized graphite nanoparticles and the physical properties of epoxy matrix nanocomposites. Compos Sci Technol 70:1120–1125
23. Choi JS, Lim ST, Choi HJ, Pozsgay A, Szazdi L (2006) Effect of interfacial interaction on the structure and rheological properties of polyamide-6/clay nanocomposites. Compos Interfaces 13:773–782
24. Gorga RE, Lau KKS, Gleason KK, Cohen RE (2006) The importance of interfacial design at the carbon nanotube/polymer composite interface. J Appl Polym Sci 102:1413–1418
25. Ma J, Meng Q, Michelmore A et al (2013) Covalently bonded interfaces for polymer/graphene composites. J Mater Chem A 1:4255–4264
26. Ma J, Meng Q, Zaman I et al (2014) Development of polymer composites using modified, high-structural integrity graphene platelets. Compos Sci Technol 91:82–90
27. Cravotto G, Cintas P (2010) Sonication-assisted fabrication and post-synthetic modifications of graphene-like materials. Chem Eur J 16:5246–5259
28. Meng Q, Zaman I, Hannam JR et al (2011) Improvement of adhesive toughness measurement. Polym Test 30:243–250
29. Katti KS, Sikdar D, Katti DR, Ghosh P, Verma D (2006) Molecular interactions in intercalated organically modified clay and clay–polycaprolactam nanocomposites: experiments and modeling. Polymer 47:403–414
30. Madejova J (2003) Vib Spectrosc 31:1
31. McMurry J (2004) Organic chemistry. Brooks/Cole, California
32. Kuan HC, Chuang WP, Ma CCM, Chiang CL, Wu HL (2005) Synthesis and characterization of a clay/waterborne polyurethane nanocomposite. J Mater Sci 40:179–185
33. Zhang K, Wang L, Wang F, Wang G, Li Z (2004) Preparation and characterization of modified-clay-reinforced and toughened epoxy–resin nanocomposites. J Appl Polym Sci 91:2649–2652
34. Gass MH, Bangert U, Bleloch AL, Wang P, Nair RR, Geim AK (2008) Free-standing graphene at atomic resolution. Nat Nanotechnol 3:676–681
35. Kornmann X, Lindberg H (2001) Synthesis of epoxy–clay nanocomposites: influence of the nature of the curing agent on structure. Polymer 42:4493–4499
36. Le QH, Kuan H-C, Dai J-B, Zaman I, Luong L, Ma J (2010) Structure–property relations of 55 nm particle-toughened epoxy. Polymer 51:4867–4879